

Polybenzimidazole-derived Carbon Molecular Sieve Membranes with “Hourglass”
Nanostructures Achieving H₂/CO₂ Separation Properties above Upper Bounds

Maryam Omidvar^{1,†}, Hien Nguyen^{1,†}, Liang Huang¹, Cara Doherty², Anita Hill², Christopher M.
Stafford³, Xianshe Feng⁴, Mark T. Swihart¹, and Haiqing Lin^{1,*}

¹Department of Chemical and Biological Engineering, University at Buffalo, The State University
of New York, Buffalo, NY 14260, USA

²Commonwealth Scientific and Industrial Research Organization (CSIRO) Manufacturing,
Private Bag 10, Clayton, South Victoria 3169, Australia

³Materials Science & Engineering Division, National Institute of Standards and Technology, MS
8542, 100 Bureau Drive, Gaithersburg, MD 20899, USA

⁴Department of Chemical Engineering, University of Waterloo, Waterloo, Ontario N2L 3G1,
Canada

[†] Equal contribution

* Corresponding author. Tel: +1-716-645-1856, Email: haiqingl@buffalo.edu (H. Lin)

Abstract

Polymers with high permeability and strong size-sieving ability are needed for H₂/CO₂ separation at temperatures ranging from 100 °C to 300 °C to enable an energy-efficient pre-combustion CO₂ capture process. However, such polymers usually suffer from a permeability/selectivity tradeoff, i.e., polymers with high selectivity tend to exhibit low gas permeability. Herein we demonstrate that carbonization of polybenzimidazole (PBI) generates desirable “hourglass” structures with microcavities (leading to high H₂ permeability) and ultra-microporous channels (leading to strong size sieving ability and thus high H₂/CO₂ selectivity). Specifically, PBI is a leading polymer for H₂/CO₂ separation with H₂ permeability of 27 Barrers (1 Barrer = 10⁻¹⁰ cm³(STP) cm cm⁻² s⁻¹ cmHg⁻¹) and H₂/CO₂ selectivity of 14 at 150 °C, while carbonization at 900 °C (CMS@900) increases the H₂ permeability to 54 Barrers and H₂/CO₂ selectivity to 80. When tested with simulated syngas containing equimolar H₂ and CO₂ in the presence of water vapor for 120 h, the CMS@900 exhibits stable H₂ permeability of ≈36 Barrers and H₂/CO₂ selectivity of ≈53 at 150 °C, which is above Robeson’s upper bound and demonstrates their potential for practical H₂ purification and CO₂ capture.

Keywords: polybenzimidazole; carbon molecular sieve membranes; H₂/CO₂ separation; free volume; CO₂ capture

Hydrogen (H₂), a large-volume commodity chemical and clean energy carrier, is mainly produced from fossil fuels via steam reforming or gasification, with carbon dioxide (CO₂) as a byproduct. CO₂ must be removed for the H₂ to be used. A sufficiently low-cost and energy-efficient H₂/CO₂ separation technology would allow CO₂ to be captured for sequestration or utilization.¹⁻³ Membrane technology has been extensively investigated for H₂/CO₂ separation due to its inherently high energy-efficiency. A key to the success of this technology is membrane materials with both high H₂ permeability and high H₂/CO₂ selectivity (preferably above 30) at syngas processing temperatures of 100 °C to 300 °C.⁴

Because H₂ has a smaller kinetic diameter than CO₂ (2.89 Å vs. 3.30 Å), the dominant strategy for designing H₂/CO₂ separation membranes aims to achieve strong size-sieving ability, using polymers (*e.g.* polybenzimidazole (PBI),^{5,6} cross-linked PBI,^{1,7} and crosslinked polyamides⁸), inorganic materials (silica,⁹ zeolites,¹⁰ metal-organic frameworks (MOFs),^{11,12} graphene oxide (GO),^{2,13} MoS₂,¹⁴ transition metal carbides and nitrides (MXenes)¹⁵), and mixed matrix membranes (MMMs) containing size-sieving inorganic fillers in polymers.¹⁶⁻¹⁸ However, the pursuit of the sharp molecular size-sieving ability often leads to low free volume and thus low H₂ permeability. This coupling of free volume and size-sieving ability leads to a permeability/selectivity tradeoff.^{1,19} An effective means of overcoming the limitations of this tradeoff is to create “hourglass” structures in materials with microcavities that promote high gas permeability and ultra-microporous channels that provide high selectivity.^{20,21} However, systematic understanding of the relationship between material chemistry, structure, and resulting properties remains insufficient to predictively design such structures, particularly for amorphous polymers (*i.e.*, the main material platform for industrial membrane gas separations). The discovery of membrane materials with structures that simultaneously provide high permeability and

selectivity is often the result of trial-and-error within classes of promising materials, such as thermally rearranged (TR) polymers²¹ and polymers of intrinsic microporosity (PIMs).²²

Recently, amorphous carbon molecular sieving (CMS) materials have been demonstrated with separation performance above the upper bound for challenging gas separations like O₂/N₂, N₂/CH₄, CO₂/CH₄, and olefin/paraffin.²³⁻²⁵ CMS materials are formed by thermal decomposition of polymer precursors and comprise parallel layers of condensed hexagonal rings without three-dimensional crystalline order. CMS materials exhibit a bimodal distribution of slit-like pores with micropores of (6 to 20) Å and ultra-micropores of less than 6 Å.^{26,27} Depending on the polymer precursors and carbonization conditions, the size of the ultra-microporous channels may be suitable for certain gas separations.²⁸⁻³⁰ For example, Matrimid[®] pyrolyzed at 800 °C shows N₂ permeability of 6.8 Barrers and N₂/CH₄ selectivity of 7.7 (which is above the upper bound for N₂/CH₄ separation), and Matrimid carbonized at 675 °C exhibits CO₂ permeability of 480 Barrers and CO₂/CH₄ selectivity of 80 (above the upper bound for CO₂/CH₄ separation).²⁷ However, the CMS membranes reported in the literature do not exhibit good H₂/CO₂ separation properties. For example, Matrimid carbonized at 675 °C provided a H₂/CO₂ selectivity of only 1.3.²⁷ Blends of PBI and Matrimid (50:50) carbonized at 800 °C exhibited H₂ permeability of 324 Barrers and H₂/CO₂ selectivity of 8.8 at 35 °C.³¹

Herein, we demonstrate, for the first time, that carbonization of PBI at optimal conditions can generate the desired hourglass structure, leading to superior H₂/CO₂ separation properties above the upper bounds at temperatures of 100 °C to 200°C. PBI is a leading material for H₂/CO₂ separation with H₂ permeability of 27 Barrers and H₂/CO₂ selectivity of 14 at 150 °C.^{1,7} The PBI carbonized at 900 °C exhibits a pure-gas H₂ permeability of 54 Barrers and H₂/CO₂ selectivity of 80 at 150 °C, which is above the Robeson's upper bound at 150 °C, and a significant improvement

over PBI itself. In this study, we thoroughly investigated the effect of carbonization temperature on the PBI-CMS structure and H₂/CO₂ separation properties and evaluated the long-term stability of the CMS films with simulated syngas (*i.e.*, gas mixtures containing water vapor) to demonstrate their potential for practical applications.

Results and discussion

Preparation and characterization of CMS films. Fig. 1a illustrates carbonization of PBI, which creates microcavities (leading to high gas permeability) and ultra-microporous channels (leading to sharp molecular sieving ability). As a result of the pyrolysis, the film color changes from yellow to black (Fig. 1b). Carbonization yields dense CMS membranes with shrinkage in both the mass and the dimensions of the precursor films. The CMS materials contain very few functional groups, as confirmed by the FTIR spectra (cf. Fig. S1 in the Supporting Information).³² The CMS samples are labeled as CMS@xxx, where xxx represents the soaking temperature (°C) used in the carbonization process.

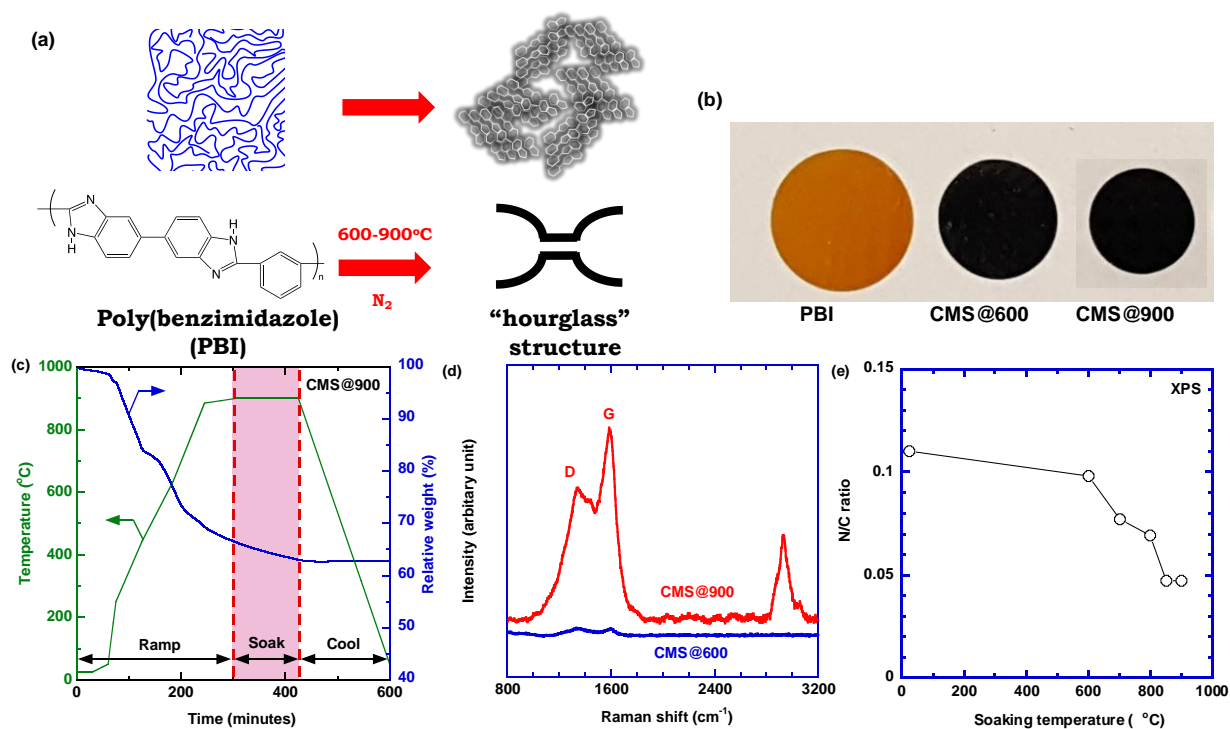


Fig. 1. Preparation and characterization of the CMS films. (a) Schematic of the carbonization of PBI to create microporous structure and ultra-microporous channels; (b) photos of PBI, CMS@600, and CMS@900 films; (c) temperature ramping and mass loss of CMS@900 monitored by TGA; (d) Raman spectra of CMS@600 and CMS@900; and (e) effect of carbonization temperature on the N/C ratio in the CMS films.

Fig. 1c shows mass loss of CMS@900 during carbonization as measured by thermogravimetric analysis (TGA). Detailed procedures for the temperature ramping and soaking, described in the Methods section of the SI, are expected to influence the microstructures of the films. PBI has a glass transition temperature (T_g) of 470 °C and a decomposition onset temperature of 500 °C. Mass loss during carbonization occurs in several steps. In the first step, below 100 °C, the film loses 1.5 mass% through evaporation of water. In a second step, from 100 °C to 450 °C, the film loses 14.5 mass% through evaporation of residual DMAc. During the third step of ramping from 450 °C to 900 °C, the PBI degrades and loses another ≈ 18 mass%. During the final soaking step, the PBI further loses ≈ 3 mass%. Therefore, the carbonization at 900 °C decreases the mass by a total of 37% for the films. Relative to the dry PBI (after the loss of water and residual solvent),

the final mass decreases by 25%. Similarly, carbonization at 600 °C decreases the mass by 24% overall, including 15% attributed to the evaporation of solvents. The mass loss relative to dry PBI is 11 % for the CMS@600 (Fig. S1).

Fig. 1d shows the Raman spectra of CMS@600 and CMS@900. The appearance of peaks at 1341 cm^{-1} and 1580 cm^{-1} confirms the formation of disordered carbon (I_D) and highly oriented graphitic carbon (I_G) in the CMS samples, respectively. CMS@900 exhibits much stronger peaks than CMS@600, confirming that higher carbonization temperatures generate more graphitized carbon. On the other hand, CMS@900 exhibits higher I_D/I_G ratio (1.5) than CMS@600 (0.87), indicating that the graphitic carbon in the CMS@900 is more defective. The graphitic crystallite size (L_a) can be estimated using Tuinstra-Koenig equation ($L_a = 4.4I_G/I_D$).^{33,34} This analysis yields the L_a value of 5.0 nm and 2.9 nm for CMS@600 and CMS@900, respectively, which is consistent with the more defective graphitic carbon in CMS@900. Fig. 1d further confirms the carbonization by elemental analysis using X-ray Photoelectron Spectroscopy (XPS). The N/C ratio decreases with increasing soaking temperature, as well as the O/C ratio (cf. Fig. S1c).

Fig. 2a shows the effect of the soaking temperature on the mass loss of the PBI samples, as monitored by TGA. Increasing the soaking temperature increases the mass loss. The mass loss can also be calculated from the mass difference of the sample before and after the carbonization. As shown in Fig. 2a, the mass loss values derived from these two methods are reasonably consistent for both CMS@600 and CMS@900.

Fig. 2b shows the effect of the soaking temperature on the bulk density (ρ_{bulk}) determined from the mass and dimension measurements of the CMS films. PBI has a density of 1.25 g/cm^3 . Carbonization first increases ρ_{bulk} before decreasing it above 750 °C, reflecting the competing effects of the generation of microcavities and growth of high-density graphite. The ρ_{bulk} values are

also compared with skeletal density ($\rho_{skeletal}$) measurements determined using helium pycnometry, which follows a similar trend with increasing soaking temperatures, except for CMS@900. The average porosity (ε) can be calculated using the following equation:³⁵

$$\varepsilon = \frac{\text{void volume}}{\text{total volume}} = 1 - \frac{\rho_{bulk}}{\rho_{skeletal}} \quad (1)$$

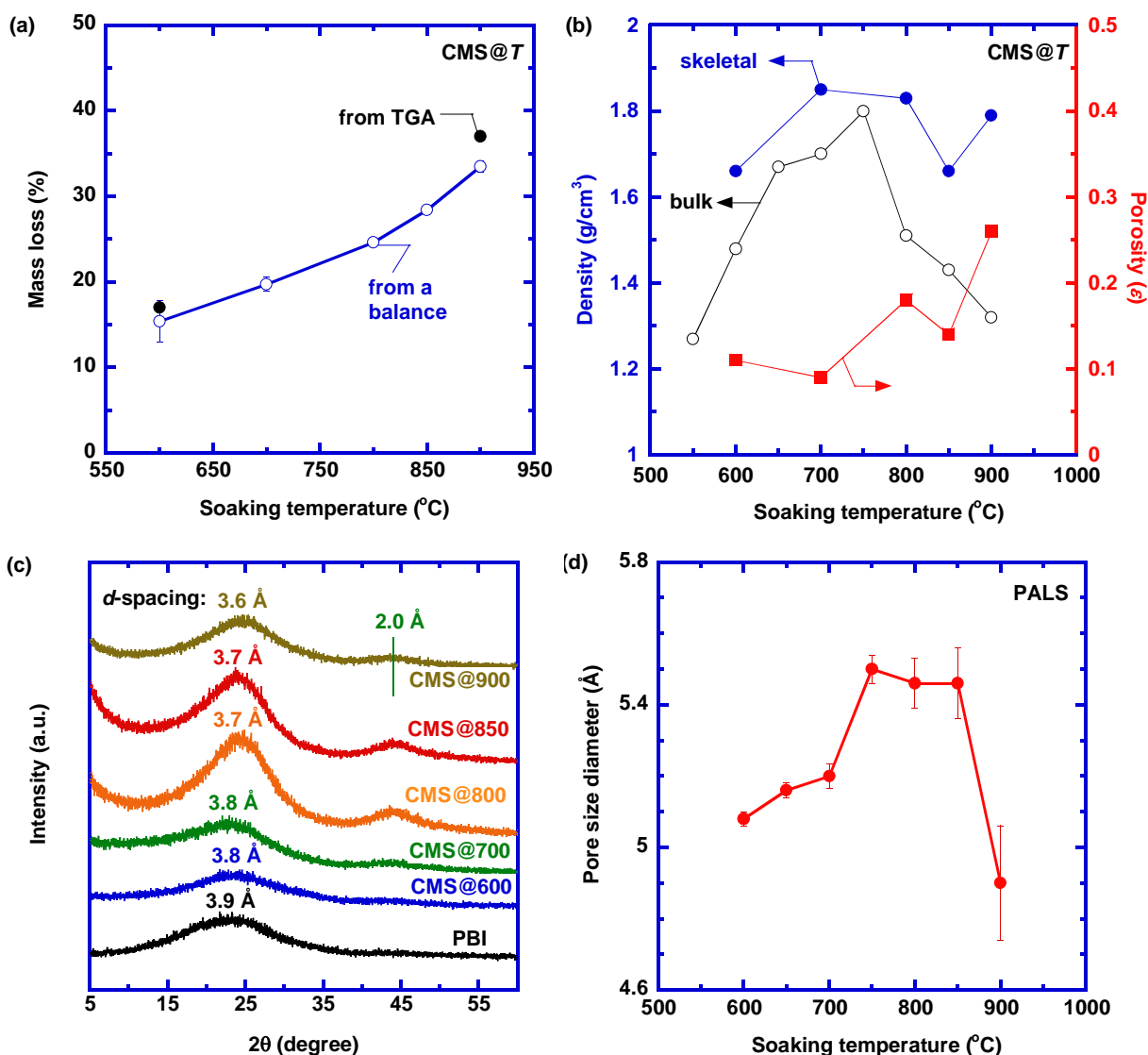


Fig. 2. Physical properties of CMS films. Effect of the soaking temperature on (a) mass loss, (b) skeletal density, bulk density, and porosity (ε), (c) Wide-angle XRD patterns and d-spacings, and (d) the diameter of free volume elements from PALS.

Increasing the carbonization temperature increases ε , consistent with the formation of microcavities in the CMS films. CMS@900 has the highest porosity of 26 %, which is very similar to that of poly(1-(trimethylsilyl)-1-propyne) (PTMSP) with a porosity of 27%, one of the most permeable polymers known.³⁶ The trend of the ε values with increasing the soaking temperature is also consistent with that for measured BET surface areas. The CMS films carbonized at temperatures below 850 °C had BET surface areas that were too low to determine, while CMS@850 and CMS@900 exhibit a BET surface area of 9 m²/g and 11 m²/g, respectively.

Fig. 2c presents the wide-angle powder X-ray diffraction (XRD) patterns for the samples carbonized at different temperatures. Carbonization decreases the d-spacing from 3.9 Å for PBI to 3.6 Å for CMS@900, suggesting the potential for increased size-sieving ability. Moreover, a small broad peak at a d-spacing of 2.0 Å appears for the CMS, which is representative of the carbon-carbon spacing in graphite planes.^{35,37}

Positron annihilation lifetime spectroscopy (PALS) was used to characterize the free volume elements in the CMS samples. The PALS technique measures the lifetimes of positron species,³⁸ such as τ_2 for a positron and an electron (no bound state formed) and τ_3 for formed ortho-positroniums (bound state of the positron and electron of the same spin). Usually, τ_3 is used to analyze the pore structure.³⁹ However, most ortho-positronium annihilations occur on the surface of the conductive CMS films, which makes it inadequate to resolve the τ_3 in the spectra. Therefore, τ_2 is used here to derive free volume characteristics.^{39,40} Fig. 3d demonstrates that increasing the soaking temperature increases the pore size before leveling off at 750 °C and then decreasing at 900 °C. With the highest porosity among the CMS samples, CMS@900 appears to have smaller pores (and sharper size-sieving ability) but a larger concentration of pores.

Pure-gas transport characteristics in CMS films. The CMS films were tested with pure-gas H₂ and CO₂ at temperatures between 35 °C and 150 °C and pressures ranging from 4.4 atm to 11 atm. The gas permeability was independent of the feed pressures. Fig. 3a presents the effect of the soaking temperature on pure-gas H₂ and CO₂ permeabilities at 100 °C and 7.4 atm. As expected, both H₂ and CO₂ permeability increase significantly after carbonizing PBI. CMS@750 exhibits H₂ permeability almost 2 orders of magnitude higher than PBI with a decrease of H₂/CO₂ selectivity from 14 to 8.7 at 100 °C because of the microcavities created. On the other hand, CMS@900 shows lower permeability and much higher selectivity than CMS@750 because of the dominant effect of densification, resulting in ultra-microporous channels with low permeability and sharp size-sieving ability. These are also consistent with the decreased d-spacing values (from WAXD) and the pore size in CMS@900 (from the PALS results).

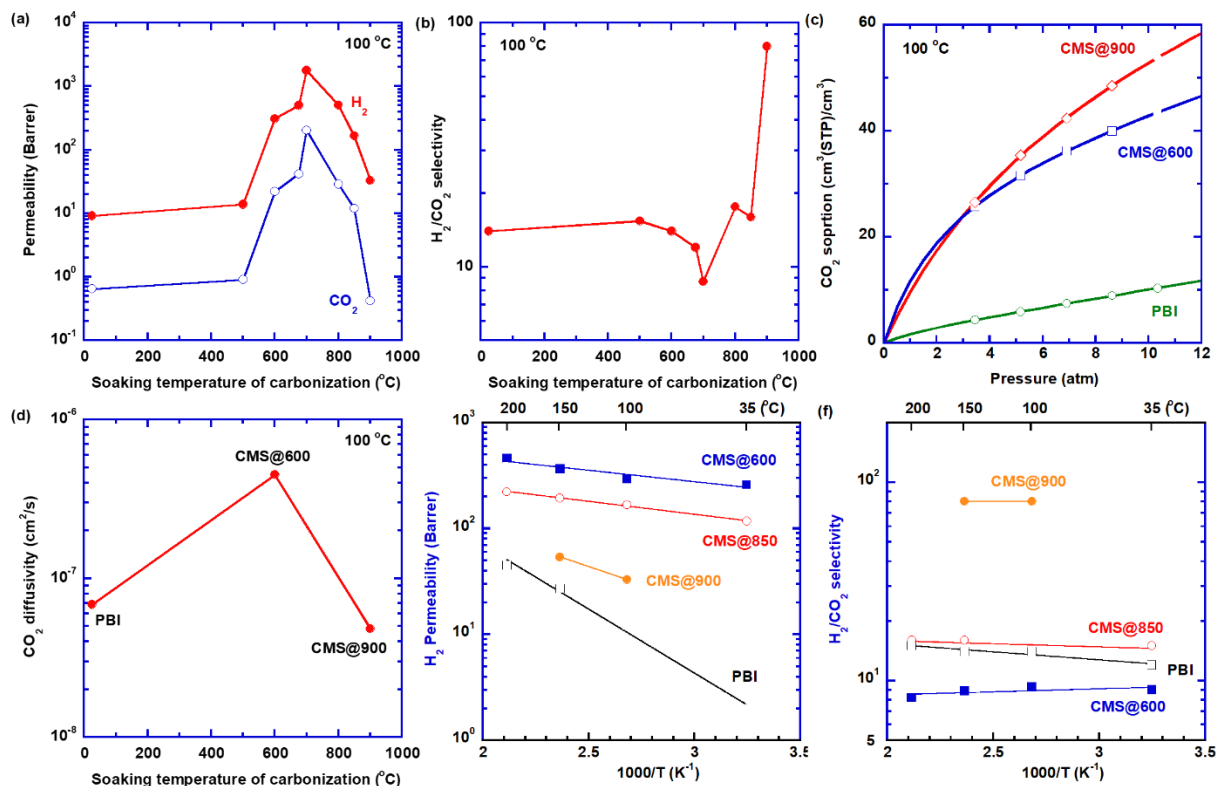


Fig. 3. Pure-gas transport characteristics. Effect of the soaking temperature in preparing the CMS films on (a) pure-gas H₂ and CO₂ permeability at 7.4 atm, and (b) H₂/CO₂ selectivity at 7.4 atm, (c) CO₂ sorption isotherms at 10 atm, and (d) CO₂ diffusivity at 10 atm and 100 °C. Effect of temperature on (e) H₂ permeability and (f) H₂/CO₂ selectivity in PBI and CMS films at 10 atm.

To elucidate the effect of carbonization on the gas transport properties, gas permeability is decoupled into solubility (S_A , cm³ (STP)/cm³ atm) and diffusivity (D_A , cm²/s). Fig. 3c presents CO₂ sorption isotherms for PBI, CMS@600, and CMS@900 at 100 °C, while H₂ solubility is below the detection limit of the apparatus. The gas sorption in CMS follows typical dual-mode sorption behavior.²⁸ Carbonization increases the CO₂ sorption because of the increase in porosity (or Langmuir's sorption capacity). For example, carbonization of PBI at 600 °C increases the CO₂ solubility from 1.0 to 4.2 cm³(STP)/cm³ atm. Fig. 3d shows the effect of carbonization on the CO₂ diffusivity at 100 °C. CMS@600 exhibits the highest CO₂ diffusivity among the three samples, reflecting the competing effect of increasing porosity (derived from microcavities) and decreasing d-spacing (related to ultra-microporous channels) with increasing the soaking temperature.

Fig. 3e displays the effect of temperature on the H₂ permeability in PBI⁷ and CMS films, which can be satisfactorily described using the Arrhenius equation. The activation energy (E_P) for H₂ permeation is also recorded in Table S3. PBI shows the highest E_P value, consistent with it having the lowest porosity, followed by CMS@900 because of its ultra-microporous structure. CMS@600 and CMS@850 show lower E_P values because of their moderate free volume size and porosity. Similar behavior is also observed for the E_P values for CO₂, as shown in Table S2. Fig. 3f demonstrates that the H₂/CO₂ selectivity is independent of temperature.

Mixed-gas H₂/CO₂ separation properties in PBI-CMS with simulated syngas. The CMS@900 exhibits the best combination of high H₂ permeability and H₂/CO₂ selectivity, and thus, it was

further evaluated with simulated syngas containing water vapor. Figs. 4a and 4b show the dependence of mixed-gas permeability and H_2/CO_2 selectivity on the CO_2 feed partial pressure at 150 °C with three H_2/CO_2 mixtures (20:80, 50:50, and 80:20). Both H_2 and CO_2 permeability (with an uncertainty of $\approx 10\%$) decrease with increasing CO_2 partial pressure due to the competitive sorption, while the mixed-gas H_2/CO_2 selectivity is independent of the CO_2 partial pressure, suggesting a lack of plasticization because of the low CO_2 sorption at 150 °C.

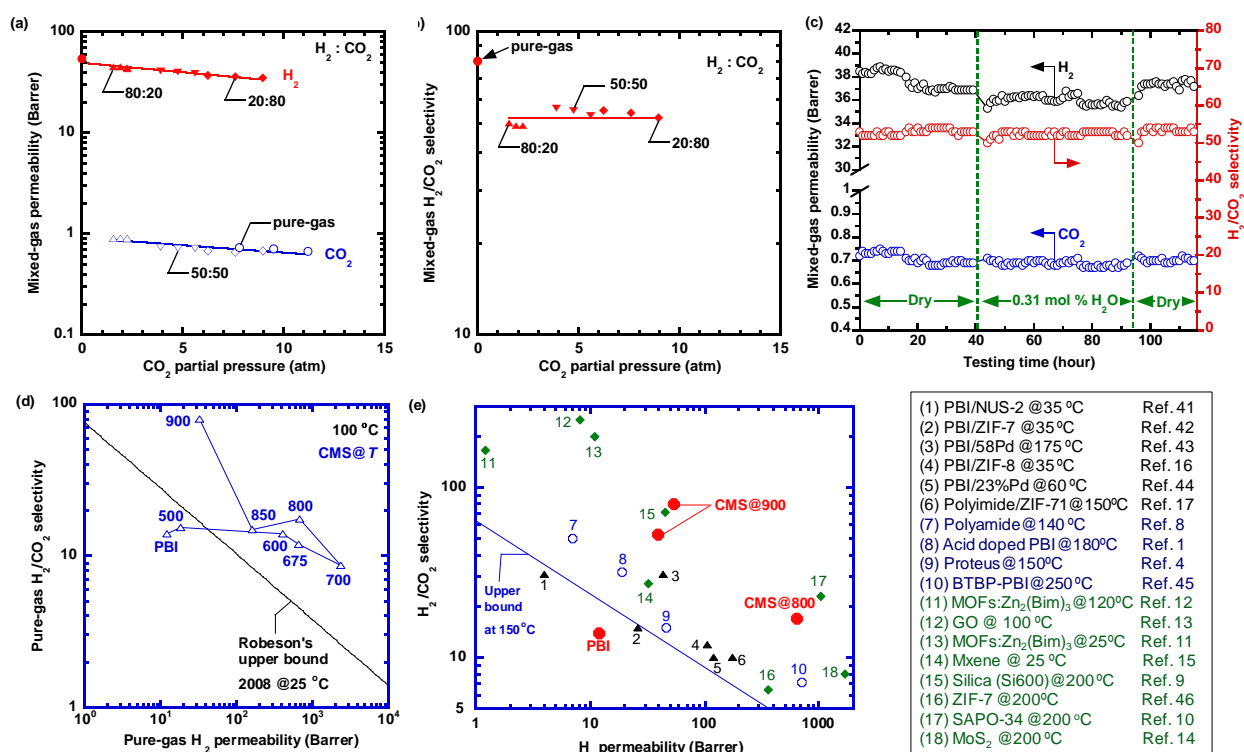


Fig. 4. H_2/CO_2 separation performance of CMS@900. Effect of the CO_2 feed partial pressure on (a) mixed-gas H_2 and CO_2 permeability, and (b) H_2/CO_2 selectivity. The lines are to guide the eye. (c) Long-term stability in dry and humidified conditions with $H_2:CO_2$ of 50:50 at 11 atm and 150 °C for 120 h. (d) Pure-gas H_2/CO_2 separation performance for various CMS samples, relative to Robeson's upper bound at 25 °C. (e) Comparison of CMS@900 with state-of-the-art materials for H_2/CO_2 separation, including MMMs,^{16,17,41-44} polymers,^{1,4,8,45} and inorganic materials.^{9-15,46}

After the water-gas shift reaction, coal-derived syngas typically contains $\approx 56\%$ H_2 , $\approx 41\%$ CO_2 , water vapor, and other light gases. Fig. 4c depicts the effect of water vapor on the mixed-gas separation properties and long-term stability of CMS@900 at 11 atm and 150 °C. The sample was

initially tested using a dry gas mixture (50 % H₂/50 % CO₂) for 40 h. Then 0.31 mol% water vapor was introduced in the feed for 54 h before switching back to the dry gas. The sample exhibits stable separation properties for 120 h with and without the water vapor.

Fig. 4d compares the H₂/CO₂ separation properties in CMS samples with the Robeson's 2008 upper bound plot.⁷ Pristine PBI shows the performance below the upper bound at 25 °C, while most CMS samples exhibit the H₂/CO₂ separation properties above the upper bound. Specifically, the CMS@900 exhibits remarkable H₂/CO₂ selectivity of 80.

Figure 4e compares the pure- and mixed-gas H₂/CO₂ separation performance of CMS@900 with a leading commercial H₂/CO₂ separation membrane (ProteusTM) in a Robeson's upper bound plot estimated for 150 °C using a transition state model.^{47,48} The CMS@900 and CMS@800 show H₂/CO₂ separation properties better than the ProteusTM materials, and significantly above the upper bound. Fig. 4e also demonstrates the superior H₂/CO₂ separation performance of CMS@900 compared with other state-of-the-art materials, including MMMs,^{16,17,41-44} polymers,^{1,4,8,45} and inorganic materials.^{9-15,46}

In summary, by choosing a suitable polymer precursor (PBI) and carbonization condition, we demonstrate for the first time that CMS membranes can be obtained with desirable structure achieving superior H₂/CO₂ separation properties above Robeson's upper bound at elevated temperatures (> 100 °C). While designing polymers with desired free volume characteristics (such as size, population, and distribution of the free volume elements) remains challenging, carbonization can provide a versatile platform to derive the required free volume characteristics in membranes for targeted separations.

Methods

General. Equipment and instruments or materials are identified herein to adequately specify the experimental details. Such identification does not imply recommendation by the National Institute of Standards and Technology, nor does it imply the materials are necessarily the best available for the purpose.

Preparation of membranes. Celazole[®] PBI (1.1 IV grade with M_w of 60,000 Da, where M_w is the mass average molecular mass) was supplied by PBI Performance Products, Inc. (Charlotte, SC), and it was first dissolved in dimethylacetamide (DMAc) at 8 % by mass and filtered using a 1.0 μm PTFE syringe filter (Thermo Fisher Scientific). Freestanding films were prepared via solution casting. After drying in a conventional oven at 80 °C for 15 h, the films were dried under vacuum at 200 °C for 48 h. The obtained films have a thickness of 100 $\mu\text{m} \pm 5 \mu\text{m}$ as measured using a Starrett 2900 digital micrometer (L.S. Starrett Co., Athol, MA).

To prepare CMS, the PBI films were pyrolyzed in a 25 mm diameter tube furnace (MTI Corporation, Richmond, CA) under 200 $\text{cm}^3(\text{STP})/\text{min}$ N_2 (ultrahigh purity) following a procedure used for the carbonization of polyimides, as shown in the SI.^{27,49} The final pyrolysis temperature (500 °C to 900 °C) was reached using a “ramp-and-soak” method, whereby the temperature ramping rate starts at 13.3 °C/min and then decreases to 3.85 °C/min and finally to 0.25 °C/min before soaking at the targeted final temperature for 2 h. Finally, the films were cooled to ≈ 23 °C in the furnace tube under flowing N_2 .

Characterization. TGA was conducted using an SDT Q600 thermogravimetric analyzer (TA Instruments, DE) under N_2 flow with temperature ramping procedures identical to those used for the carbonization of membranes. Attenuated total reflection-Fourier transform infrared (ATR-FTIR) spectra were collected using a Bruker Vertex 70 spectrometer (Billerica, MA). For each sample, 100 scans were recorded at a resolution of 4.0 cm^{-1} at ≈ 21 °C. XPS was used for elemental

analysis of the PBI and CMS films. A Kratos AXIS Ultra DLD Spectrometer (Kratos Analytical, Manchester, UK) was used at the chamber pressure of $\approx 1.33 \times 10^{-7}$ Pa. The spectra were obtained from a nominal spot size of $300 \mu\text{m} \times 700 \mu\text{m}$ and analyzed using the CasaXPS software package.

The density of the freestanding films was determined from their mass and volume. The volume was calculated from the film thickness and area (which leads to the bulk density) or measured using a Micromeritics Accu-Pyc II 1340 Gas Pycnometer (Micromeritics Instrument Corporation, Norcross, GA), which leads to the skeletal density. WAXD patterns of the CMS films were collected using a Rigaku Ultima IV x-ray diffractometer over a 2θ range of 5° to 45° with a scanning rate of $2.0^\circ \text{ min}^{-1}$. The diffractometer has a Cu $K\alpha$ x-ray source with a wavelength of 1.54 \AA . Surface area of CMS films were determined using Micromeritics Tri-Star II with VacPrep. PALS was used to determine the free volume characteristics of the CMS films under vacuum (1×10^{-5} Torr) at $\approx 22^\circ \text{C}$ using an EG&G Ortec (Oak Ridge, TN) fast-fast coincidence spectrometer.

Pure-gas permeability was determined using a constant-volume/variable-pressure apparatus at controlled temperatures.⁴⁸ Mixed-gas permeability was determined using a constant-pressure/variable-volume apparatus with a sweep gas of N_2 .¹ Binary mixtures were prepared by in-line mixing of pure H_2 and CO_2 streams at desired flow rates. Water vapor was introduced by passing the mixed gas through a water bubbler. The composition of each stream was analyzed by a model 3000 Micro GC gas analyzer (Inficon Inc., Syracuse, NY). The permeability typically has an uncertainty of $\approx 10\%$, estimated using propagation of errors.⁵⁰ Gas solubility in CMS films was determined using a microbalance (IGA 001, Hiden Isochema, Warrington, UK) at various temperatures and pressures. The gas sorption was calculated using the mass change of the samples ($\approx 100 \text{ mg}$) after gas sorption reached equilibrium, accounting for buoyancy effects.^{1,7} The uncertainty of the gas solubility is estimated to be $\approx 10\%$ using propagation of error analysis.⁵⁰

Acknowledgments

We acknowledge the financial support of the U.S. National Science Foundation (NSF) under award #1554236 and the U.S. Department of Energy (DOE) under award #DE-FE0031636. C.M.D. acknowledges support from the ARC (Award No. DE1401359) and the Veski Inspiring Women fellowship.

Author contributions

H.L. and M.O. conceived the project and designed experiments. M.O., H.N., and L.H. prepared and characterized the CMS samples. C.M.D. and A.J.H. performed the PALS measurement. C.M.S. performed the XPS analysis. All the authors analyzed and interpreted data. M.O. and H.L. wrote the manuscript. All the authors discussed the results and commented on the manuscript.

Data availability. The data that support the findings of this study are available from the corresponding author upon request.

References

- 1 Zhu, L., Swihart, M. T. & Lin, H. Unprecedented size-sieving ability in polybenzimidazole doped with polyprotic acids for membrane H₂/CO₂ separation. *Energy Environ. Sci.* **11**, 94-100, (2018).
- 2 Kim, H. *et al.* Selective gas transport through few-layered graphene and graphene oxide membranes. *Science* **342**, 91-95, (2013).
- 3 Lin, H., Van Wagner, E., Freeman, B. D., Toy, L. G. & Gupta, R. P. Plasticization-enhanced H₂ purification using polymeric membranes. *Science* **311**, 639-642, (2006).
- 4 Merkel, T. C., Zhou, M. & Baker, R. W. Carbon dioxide capture with membranes at an IGCC power plant. *J. Membr. Sci.* **389**, 441-450, (2012).

- 5 Berchtold, K. A., Singh, R. P., Young, J. S. & Dudeck, K. W. Polybenzimidazole composite membranes for high temperature synthesis gas separations. *J. Membr. Sci.* **415-416**, 265-270, (2012).
- 6 Joseph, R. M. *et al.* Synthesis and characterization of polybenzimidazole membranes for gas separation with improved gas permeability: A grafting and blending approach. *J. Membr. Sci.* **564**, 587-597, (2018).
- 7 Zhu, L., Swihart, M. T. & Lin, H. Tightening polybenzimidazole (PBI) nanostructure via chemical cross-linking for membrane H₂/CO₂ separation. *J. Mater. Chem. A* **5**, 19914-19923, (2017).
- 8 Ali, Z. *et al.* Ultra-selective defect-free interfacially polymerized molecular sieve thin-film composite membranes for H₂ purification. *J. Mater. Chem. A* **6**, 30-35, (2018).
- 9 de Vos, R. M. & Verweij, H. High-selectivity, high-flux silica membranes for gas separation. *Science* **279**, 1710-1711, (1998).
- 10 Yu, M., Funke, H. H., Noble, R. D. & Falconer, J. L. H₂ separation using defect-free, inorganic composite membranes. *J. Am. Chem. Soc.* **133**, 1748-1750, (2011).
- 11 Peng, Y. *et al.* Metal-organic framework nanosheets as building blocks for molecular sieving membranes. *Science* **346**, 1356-1359, (2014).
- 12 Peng, Y., Li, Y., Ban, Y. & Yang, W. Two-dimensional metal-organic framework nanosheets for membrane-based gas separation. *Angew. Chem. Int. Ed.* **56**, 9757-9761, (2017).
- 13 Li, H. *et al.* Ultrathin, molecular-sieving graphene oxide membranes for selective hydrogen separation. *Science* **342**, 95-98, (2013).
- 14 Achari, A., S, S. & Eswaramoorthy, M. High performance MoS₂ membranes: effects of thermally driven phase transition on CO₂ separation efficiency. *Energy Environ. Sci.* **9**, 1224-1228, (2016).
- 15 Shen, J. *et al.* 2D MXene nanofilms with tunable gas transport channels. *Adv. Funct. Mater.* **28**, 1801511, (2018).
- 16 Yang, T., Shi Gui, M. & Chung, T.-S. Symmetric and asymmetric zeolitic imidazolate frameworks (ZIFs)/polybenzimidazole (PBI) nanocomposite membranes for hydrogen purification at high temperatures. *Adv. Energy Mater.* **2**, 1358-1367, (2012).
- 17 Japip, S., Liao, K.-S. & Chung, T.-S. Molecularly tuned free volume of vapor cross-linked 6FDA-durene/ZIF-71 MMMs for H₂/CO₂ separation at 150 °C. *Adv. Mater.* **29**, 1603833, (2016).
- 18 Wang, Z., Wang, D., Zhang, S., Hu, L. & Jin, J. Interfacial design of mixed matrix membranes for improved gas separation performance. *Adv. Mater.* **28**, 3399-3405, (2016).
- 19 Park, H. B., Kamcev, J., Robeson, L. M., Elimelech, M. & Freeman, B. D. Maximizing the right stuff: The trade-off between membrane permeability and selectivity. *Science* **356**, (2017).
- 20 Freeman, B. D. Basis of permeability/selectivity tradeoff relations in polymeric gas separation membranes. *Macromolecules* **32**, 375-380, (1999).
- 21 Park, H. B. *et al.* Polymers with cavities tuned for fast selective transport of small molecules and ions. *Science* **318**, 254-258, (2007).
- 22 Carta, M. *et al.* An efficient polymer molecular sieve for membrane gas separations. *Science* **339**, 303-307, (2013).
- 23 Sanyal, O. *et al.* Next generation membranes—using tailored carbon. *Carbon* **127**, 688-698, (2018).

- 24 Koros, W. J. & Zhang, C. Materials for next-generation molecularly selective synthetic membranes. *Nat. Mater.* **16**, 289-297, (2017).
- 25 Park, H. B. & Lee, Y. M. Fabrication and characterization of nanoporous carbon/silica membranes. *Adv. Mater.* **17**, 477-483, (2005).
- 26 Adams, J. S. *et al.* New insights into structural evolution in carbon molecular sieve membranes during pyrolysis. *Carbon* **141**, 238-246, (2019).
- 27 Rungta, M. *et al.* Carbon molecular sieve structure development and membrane performance relationships. *Carbon* **115**, 237-248, (2017).
- 28 Fu, S. L., Sanders, E. S., Kulkarni, S. S. & Koros, W. J. Carbon molecular sieve membrane structure-property relationships for four novel 6FDA based polyimide precursors. *J. Membr. Sci.* **487**, 60-73, (2015).
- 29 Park, H. B., Kim, Y. K., Lee, J. M., Lee, S. Y. & Lee, Y. M. Relationship between chemical structure of aromatic polyimides and gas permeation properties of their carbon molecular sieve membranes. *J. Membr. Sci.* **229**, 117-127, (2004).
- 30 Fu, S. L. *et al.* Effects of pyrolysis conditions on gas separation properties of 6FDA/DETDA:DABA(3:2) derived carbon molecular sieve membranes. *J. Membr. Sci.* **520**, 699-711, (2016).
- 31 Hosseini, S. S. & Chung, T. S. Carbon membranes from blends of PBI and polyimides for N₂/CH₄ and CO₂/CH₄ separation and hydrogen purification. *J. Membr. Sci.* **328**, 174-185, (2009).
- 32 Das, M., Perry, J. D. & Koros, W. J. Effect of processing on carbon molecular sieve structure and performance. *Carbon* **48**, 3737-3749, (2010).
- 33 Ferrari, A. C. & Basko, D. M. Raman spectroscopy as a versatile tool for studying the properties of graphene. *Nat. Nanotechnol.* **8**, 235, (2013).
- 34 Abeykoon, N. C. *et al.* Novel binder-free electrode materials for supercapacitors utilizing high surface area carbon nanofibers derived from immiscible polymer blends of PBI/6FDA-DAM: DABA. *RSC Adv.* **7**, 20947-20959, (2017).
- 35 Vu, D., Koros, W. J. & Miller, S. J. High pressure CO₂/CH₄ separation using carbon molecular sieve hollow fiber membranes. *Ind. Eng. Chem. Res.* **41**, 367-380, (2002).
- 36 Volkov, A. *et al.* Liquid permeation through PTMSP: One polymer for two different membrane applications. *J. Membr. Sci.* **440**, 98-107, (2013).
- 37 Geiszler, V. C. & Koros, W. J. Effects of polyimide pyrolysis conditions on carbon molecular sieve membrane properties. *Ind. Eng. Chem. Res.* **35**, 2999-3003, (1996).
- 38 Rowe, B. W. *et al.* A variable energy positron annihilation lifetime spectroscopy study of physical aging in thin glassy polymer films. *Polymer* **50**, 6149-6156, (2009).
- 39 Geise, G. M., Doherty, C. M., Hill, A. J., Freeman, B. D. & Paul, D. R. Free volume characterization of sulfonated styrenic pentablock copolymers using positron annihilation lifetime spectroscopy. *J. Membr. Sci.* **453**, 425-434, (2014).
- 40 Rungta, M., Xu, L. & Koros, W. J. Structure–performance characterization for carbon molecular sieve membranes using molecular scale gas probes. *Carbon* **85**, 429-442, (2015).
- 41 Kang, Z. *et al.* Mixed Matrix Membranes (MMMs) Comprising Exfoliated 2D Covalent Organic Frameworks (COFs) for Efficient CO₂ Separation. *Chem. Mater.* **28**, 1277-1285, (2016).
- 42 Yang, T., Xiao, Y. & Chung, T.-S. Poly-/metal-benzimidazole nano-composite membranes for hydrogen purification. *Energy Environ. Sci.* **4**, 4171-4180, (2011).

- 43 Zhu, L. *et al.* Sorption-Enhanced Mixed Matrix Membranes with Facilitated Hydrogen
Transport for Hydrogen Purification and CO₂ Capture. *Submitted*, (2019).
- 44 Villalobos Luis, F., Hilke, R., Akhtar Faheem, H. & Peinemann, K.-V. Fabrication of
polybenzimidazole/palladium nanoparticles hollow fiber membranes for hydrogen
purification. *Adv. Energy Mater.* **8**, 1701567, (2017).
- 45 Li, X., Singh, R. P., Dudeck, K. W., Berchtold, K. A. & Benicewicz, B. C. Influence of
polybenzimidazole main chain structure on H₂/CO₂ separation at elevated temperatures. *J.*
Membr. Sci. **461**, 59-68, (2014).
- 46 Li, Y.-S. *et al.* Molecular sieve membrane: Supported metal–organic framework with high
hydrogen selectivity. *Angew. Chem. Int. Ed.* **122**, 558-561, (2010).
- 47 Rowe, B. W., Robeson, L. M., Freeman, B. D. & Paul, D. R. Influence of temperature on
the upper bound: Theoretical considerations and comparison with experimental results. *J.*
Membr. Sci. **360**, 58-69, (2010).
- 48 Omidvar, M., Stafford, C. M. & Lin, H. Thermally stable cross-linked P84 with superior
membrane H₂/CO₂ separation properties at 100° C. *J. Membr. Sci.* **575**, 118-125, (2019).
- 49 Ning, X. & Koros, W. J. Carbon molecular sieve membranes derived from Matrimid®
polyimide for nitrogen/methane separation. *Carbon* **66**, 511-522, (2014).
- 50 Bevington, P. R. & Robinson, D. K. *Data Reduction and Error Analysis for the Physical
Sciences*. 2nd edn, (McGraw-Hill, Inc., 1992).